HHS Public Access

Author manuscript

Curr Biol. Author manuscript; available in PMC 2015 August 18.

Published in final edited form as:

Curr Biol. 2014 August 18; 24(16): 1909–1917. doi:10.1016/j.cub.2014.07.001.

Matrix elasticity regulates lamin-A,C phosphorylation and turnover with feedback to actomyosin

Amnon Buxboim[1,2,*], **Joe Swift**[1,*], **Jerome Irianto**[1], **Kyle R. Spinler**[1], **P. C. Dave P. Dingal**[1], **Avathamsa Athirasala**[1], **Yun-Ruei C. Kao**[1], **Sangkyun Cho**[1], **Takamasa Harada**[1], **Jae-Won Shin**[1], and **Dennis E. Discher**[1,2,**]

[1]Molecular and Cell Biophysics Lab, University of Pennsylvania, Philadelphia, PA 19104

[2]Physics and Astronomy, University of Pennsylvania, Philadelphia, PA 19104

Summary

Tissue microenvironments are characterized not only in terms of chemical composition but also by collective properties such as stiffness, which influences the contractility of a cell, its adherent morphology, and even differentiation [1–8]. The nucleoskeletal protein lamin-A,C increases with matrix stiffness, confers nuclear mechanical properties, and influences differentiation of mesenchymal stem cells (MSCs) [9]. Here we show in single cell analyses that matrix stiffness couples to myosin-II activity to promote lamin-A,C *de*phosphorylation at Ser22, which regulates turnover, lamina physical properties, and actomyosin expression. Lamin-A,C phosphorylation is low in interphase versus dividing cells and its levels rise with states of nuclear rounding in which myosin-II generates little to no tension. Phosphorylated lamin-A,C localizes to nucleoplasm, and phosphorylation is enriched on lamin-A,C fragments and is suppressed by a cyclin-dependent kinase (CDK) inhibitor. Lamin-A,C knockdown in primary MSCs suppresses transcripts predominantly among actomyosin genes, especially in the Serum Response Factor (SRF) pathway. Levels of myosin-IIA thus parallel levels of lamin-A,C, with phosphosite mutants revealing a key role for phospho-regulation. In modeling the system as a parsimonious gene circuit, tension-dependent stabilization of lamin-A,C and myosin-IIA is shown to suitably couple nuclear and cell morphology downstream of matrix mechanics.

Results and discussion

Lamin-A,C phosphorylation in interphase cells is favored by low nuclear stress

The inner nuclear membrane is lined by juxtaposed networks of two types of intermediate filament proteins. The main products of the *LMNA* gene, lamin-A and the truncated spliceform lamin-C, have long been known to vary greatly between different tissues [10]. *LMNB1* is the founding member of the intermediate filament superfamily [11] that also

**Corresponding author: discher@seas.upenn.edu; telephone: (+1) 215-898-4809.
*Equal contributions.

includes *LMNB2* which varies minimally in expression between different tissues [9]. The lamina interacts with numerous nuclear proteins and chromatin as well as linking across the nuclear envelope to the cytoskeleton [12–14]. Our recent proteomics analyses of tissue samples and cells showed that lamin-A,C (LMNA) is unique among these various factors in increasing systematically with tissue stiffness [9]. We further showed with cultured cells that lamin-A,C increases with matrix stiffness and can enhance differentiation, although the molecular basis for mechano-regulation was unclear. Mass spectrometry (MS) of bulk lysates suggested lamin-A,C was more phosphorylated on soft matrices than stiff matrices, but lamin-A,C phosphorylation is also abundant in rounded mitotic cells (uncaging the chromatin). One of the best characterized phosphorylation sites in lamin-A,C is Ser22 [15, 16], for which there is an antibody suitable for high resolution cell imaging, and so we hypothesized that pSer22 in interphase cells would be highest in states of low cell tension.

Quantitative immunofluorescence showed pSer22 in the nuclei of every cell (Figs. 1A; S1A–C); amounting to ~ 5–10% of total lamin-A,C as calibrated by synthetic peptides using MS (Figs. 1B; S1D, E). Intensities in each interphase nucleus were at least several-fold above the intensity of the secondary antibody control (Fig. S1B) while also ~10-fold less than in dividing cells (Figs. 1B, S1C, D). Specificity of anti-pSer22 was confirmed with an epitope blocking phospho-peptide that greatly decreased signal in both non-dividing nuclei and dividing cell cytoplasm (Fig. 1B). Lamin-A,C is thus phosphorylated at Ser22 during interphase.

MSCs were seeded from suspension onto soft (0.3kPa) or stiff (40kPa) matrices, and then fixed and imaged at various time points. The fraction of lamin-A,C phosphorylated at Ser22 (pSer22/LMNA) decreased concomitantly with greater nuclear spreading and total lamin-A,C, which were both promoted by stiff matrix (Fig. 1C). Cells cultured on a very thin layer (3–15 μm) of soft matrix on top of glass exhibited behavior intermediate between cells on soft and stiff gels (both > 35 μm thick), and indeed in the case of total lamin-A,C and pSer22/LMNA, the soft/thin gel behaved most like the stiff/thick gel. The soft/thin gel had the same chemical composition as the thicker soft gel, but the proximity of the hard glass substrate increases the apparent stiffness ‘felt’ by the cell so that hydrogel composition seems unimportant [17, 18]. After 24 hrs, lamin-A,C de-phosphorylation on soft gels was half that on stiff matrices, but changes in phosphorylation were observed within hours of cell adhesion, which is similar in time scale to changes in lamin-A,C level and nuclear spreading. Rapid post-translational changes under stress have been reported in other mechanotransduction pathways such as p130Cas when extended by cell tension to expose sites for phosphorylation [4]. For lamin-A,C in isolated nuclei, we have recently demonstrated stress-modulation of a site-specific, non-enzymatic modification (i.e. fluorophore conjugation to a buried cysteine) [9], and so stress-modulation of lamin-A,C phosphorylation could likewise depend on stress-modulation of lamin-A,C’s structure. However, here where we focus on the important downstream consequences of phosphorylated lamin-A,C after providing further evidence of a stress-modulated mechanism.

Upon detachment from substrate into suspension, MSCs and their nuclei rapidly rounded as cytoskeletal tension was relaxed. This process was accompanied within tens of minutes by

lamin-A,C phosphorylation at Ser22 (Fig. 1D). Cytoskeletal tension was similarly relaxed by treatment with the myosin-II inhibitor blebbistatin (blebb), resulting in a reduction in nuclear spread area and increased pSer22/LMNA (Figs. 1E; S1E). Knockdown (KD) of myosin-IIA also increased pSer22/LMNA (Fig. S1F) and expression of a phosphomimetic myosin-IIA construct, S1943D, known to suppress stress fiber assembly [19, 20], lowered the amount of lamin-A,C (Fig. S1G). Matrix mechanics, cell detachment or re-attachment, cell spreading and myosin inhibition all collectively and independently support the conclusion that low nuclear stress favors lamin-A,C phosphorylation.

A nominal ‘nuclear tension’ in cell spreading was estimated from the product of nuclear strain and nuclear stiffness, as calculated respectively from the fold-change in projected nuclear area (Fig. 1F) and from the level of lamin-A,C which contributes to stiffness (see Supplementary Information). Re-plotting the pSer22/LMNA values for matrix-dependent MSC spreading (Fig. 1C) and blebb treatment (Fig. 1E) versus nuclear tension collapsed all of the data onto hyperbolic decays, consistent with inhibition of lamin-A,C phosphorylation by nuclear tension (Figs. 1G, H).

Lamin-A phosphomutants moderate nuclear mechanosensitivity

To assess the functional importance and properties of lamin-A,C phosphorylation, MSCs were transfected with GFP-fusions of lamin-A having either a phospho-mimetic S22D or a non-phosphorylatable S22A and compared to cells transfected with WT GFP-lamin-A. Fluorescence recovery after photobleaching (FRAP, Fig. 2A) was used to assess the mobile fractions *f* (at 5–10 min) of the S22 variant proteins during and after cell attachment to soft and stiff substrates. FRAP was started 30 min after plating cells, and blebb was added after 24 hrs. Up to 30–40% of WT GFP-lamin-A was mobile 30 min after plating, regardless of matrix stiffness (Fig. S2A). However, lamin-A was progressively immobilized with cell adhesion, and by just 2 hrs (with $\tau \approx 1$ hr) the soluble fraction was a stable ~15% on soft matrix and <5% on stiff matrix. The higher mobility of WT GFP-lamin-A in rounded nuclei on soft matrix at both 2 hr and 24 hr, and also following inhibition of contractility with blebb treatment, (Fig. 2B) was consistent with higher pSer22 (Figs. 1C, E). The findings are also consistent with the fact that during cell division the phosphorylation of Ser22 solubilizes lamin-A,C [15].

In contrast to WT lamin-A, neither S22D nor S22A exhibited a dependence of mobile fraction *f* on matrix stiffness (Figs. 2B; S2B). Phosphorylation of lamin-A thus appeared downstream of matrix. Moreover, S22D mobility remained high four-fold longer than WT ($\tau \approx 4$ hrs), regardless of stiffness. Although by 24 hrs *f* was similar for S22D and WT on soft gels, perhaps due to phosphorylation of sites other than Ser22, blebb had no significant effect on *f* for S22D. Since S22A lamin-A was completely immobilized after only 2 hrs of adhesion to any matrix (Fig. S2B), the phospho-dynamics of Ser22 seemed important to lamin-A,C mobility. A similar increase in mobile fraction for phosphomimetic S22E lamin-A over WT and S22A was observed in lung carcinoma A549 cells (Fig. S2C).

While ectopically expressed WT GFP-LMNA localized predominantly at the nuclear envelope, as did S22A, the phospho-mimetic S22D appeared more homogenous within MSC nuclei (Fig. 2C – top). A diffuse nuclear distribution of S22D was consistent with confocal

Z-stack imaging that showed nucleoplasmic pSer22 staining in fixed MSCs (Fig. 2C – bottom). Live cell imaging showed that both S22D and S22A completely suppressed differences in nuclear area between cells on soft and stiff matrices: while the WT expressing cells had twice the nuclear area on stiff vs. soft matrix, S22D suppressed nuclear spreading on stiff matrix and S22A suppressed nuclear rounding on soft matrix (Fig. 2D). The morphological and molecular-structural characteristics of S22 phosphomutants were also accompanied by significant changes in nuclear deformability (Fig. 2E): the relaxation times of micropipette-aspirated nuclei at fixed stress showed softening of S22D nuclei and stiffening with S22A, relative to WT. The phospho-dynamics of S22 in lamin-A,C are thus critical in determining the structural organization and mechanics of nuclei during cell spreading.

Lamin-A,C degradation is downstream of phosphorylation

During cell division comprehensive phosphorylation is required to disassemble the lamina, but during interphase, our results suggest that cells titrate lamin-A,C levels and phosphorylation to regulate molecular mobility and nuclear stiffness in proportion to cytoskeletal stress and matrix stiffness. We hypothesized that these processes were linked, with high pSer22 in relaxed cells favoring lamin-A,C degradation. Full lane immunoblots of lamin-A,C in MSCs maintained in suspension in serum-supplemented media for 10 or 45 min showed a decrease in intact lamin-A,C with time and slightly increased intensity of weak lower bands (Fig. 3A). Immunostaining of the same blots for pSer22 revealed the same bands plus many additional lower bands, with densitometry illustrating the differences (Figs. 3B; S3A, B). To confirm specificity of the antibody, gels were sliced for Mass Spectrometry analyses, and the lower MW bands indeed yielded up to 28 distinct lamin-A,C derived peptides (Figs. 3C, D; S3C). Lamin-A,C peptides were found in each of the lower molecular weight gel slices from lysates of MSCs and A549 cells (Figs. 3D; S3D). Immunoblotting with antibody against cleaved lamin-A also revealed an abundance of signal at low MW with very little signal from intact protein (Fig. 3E). Immunoblot analyses – as with any bulk technique – could reflect distinct subpopulations of cells, but immuno-fluorescence imaging demonstrated that anti-pSer22, as well as monoclonal and polyclonal antibodies against anti-cleaved lamin-A, produced significant signal in every nucleus (Fig. S3F).

To assess whether degradation could be downstream of phosphorylation, we leveraged the fact that lamin-A,C is classically a target of cyclin-dependent kinases (CDKs). MSCs were treated with an inhibitor, RO3306, shown to act against several CDKs at μM concentration [22]; treatments of ≤ 6 hrs tend to minimize extraneous changes in protein levels. In drug-treated cells, quantitative immunofluorescence revealed a ~ 50% decrease in pSer22 and > 80% decrease in immunostaining of cleaved lamin-A,C, as assessed with two independent antibodies (Figs. 3F,G; S3F). Drug-treated cells also showed higher lamin-A,C and larger nuclear areas consistent with a high-contractility phenotype induced by phospho-inhibition (Fig. S3G). Additionally, plotting pSer22/LMNA as a function of nuclear tension (as in Figs. 1G, H) fit to an appropriate hyperbolic form (Fig. S3H). Since the CDK inhibitor suppressed lamin-A,C phosphorylation and degradation, we expected that drug-treated nuclei would also be stiffer in micropipette aspiration; indeed, the nuclear relaxation times were ~ 10,000

fold longer than untreated cells (Fig. 3H). Phosphorylation of lamin-A,C thus precedes turnover and nuclear softening.

Correlated phosphorylation of S390 and S22 sites in lamin-A,C

A large number of lamin-A,C phospho-sites have been identified by MS, with many occurring in mitosis [23–25]. Our earlier MS studies identified Ser22, Ser390, Ser404 and Thr424 as more phosphorylated on soft compared to stiff substrate [9], and recent work has associated phosphorylation of Ser404 with turnover of lamin-A precursor [26]. While the well-studied pSer22 modification is recognized by commercial antibodies, MS analyses of multiple samples showed that over-expression of lamin-A resulted in greater phosphorylation of both Ser22 and Ser390 (Fig. 3I). The addition here of excess lamin-A, perturbing the mechanical equilibrium of the cell and conceivably relieving or disrupting tension on the nucleoskeleton, is perhaps compensated for in the cell by increased phosphorylation and subsequent lamin turnover. Conversely, lamin-A,C KD resulted in reduced phosphorylation at both sites, thus helping to maintain the integrity of the diminished lamina (Fig. 3J). Furthermore, titration with synthetic peptides showed Ser390 to be phosphorylated 1–5 % in both A549 cells and MSCs (Fig. S1E). Ser404 and Thr424 modifications were not detected in these experiments, suggestive of lower frequency of modification per molecule.

Lamin-A,C level and phospho-mutants regulate myosin-IIA

Since the phosphomimetic mutant of lamin-A,C led to nuclear rounding, and since lamin-A,C interacts with nuclear actin and actin-binding proteins [27, 28] to partially regulate at least a few components in the SRF pathway [9, 29], we hypothesized broad control of acto-myosin gene expression [30]. Whole genome transcriptional profiling of *LMNA* KD MSCs showed repression of target genes and cofactors of the mechanosensitive SRF pathway (Figs. 4A, B), leading to broad suppression of the actin cytoskeleton to a greater extent than any other pathways (Fig. S4A). Proteomic profiles showed excellent correlation with transcript profiles, with all significantly altered SRF targets, including myosin-IIA (*MYH9* gene), repressed at both protein and mRNA level (Fig. 4C).

To investigate a functional link between lamin-A,C phosphorylation and myosin-IIA (MYH9), A549 cell lines were established with shRNA knockdown of endogenous lamin-A,C plus transduction with GFP-lamin-A constructs WT, S22E and S22A (Figs. 4D; S4B–D). Overexpression of lamin-A generally increased myosin-IIA above a basal level (Fig. 4E), and at higher overexpression levels of the non-phosphorylatable and immobile S22A construct, myosin-IIA increased to a much greater extent compared to overexpression of phosphomimetic S22E. A hyperbolic fit to the S22A data intercepted the y-axis at a non-zero value, suggesting that a fraction of myosin-IIA expression is independent of lamin-A,C consistent with the presence of this essential myosin in lamin-A,C knockout mice [31, 32]. Since lamin-A,C primarily regulates the actomyosin cytoskeleton, depolymerization of F-actin in our studies of nuclear stiffness (see Methods) as modulated by lamin-A,C phosphorylation (Figs. 2E, 3H) seems likely to reveal properties attributable directly to the structural state of lamin-A,C.

Systems Mechanobiology Gene Circuit (MGC) couples lamin-A,C and myosin-IIA expression

While our recent work established that lamin-A,C positively regulated its own transcription factor [9], lamin-A,C phospho-dynamics here affect also myosin-IIA levels. Based on these and additional experimental insights, a parsimonious model of expression and degradation for both lamin-A,C and myosin-IIA message and protein was formulated as a 'mechanobiological gene circuit' (MGC) (Fig. 4F and Supplemental Information) in order to assess with a stably coupled system could be reasonably achieved. The most important and atypical aspect of the model is mechanically regulated degradation of these two structural proteins, which follows otherwise standard cooperative Michaelis-Menten type enzyme kinetics. Transcription of both genes was assumed to be linear in lamin-A,C protein, and linearity was also assumed for degradation of transcript as well as for protein synthesis. Equations describing the MGC were solved numerically, constrained by experimental observations (Figs. 1G, H and Supplemental Information), and the nonlinear degradation terms fed back into the gene circuit to generate stable expression states of both lamin-A,C and myosin-IIA (Fig. 4G). As matrix stiffness and cell tension suppressed protein phosphorylation and turnover (modeled from relations in the MGC in Fig. 4H), steady state levels monotonically increased with matrix *E*, consistent with coupled mechano-regulation of lamin-A,C and myosin-IIA. With this initial model in hand, further experiments will be needed to measure the stress-dependent rate constants for the lamins and many other relevant proteins, and fortunately there are now high throughput methods of sequencing and proteomics that seem appropriate [33].

Experimental procedures

Additional details of the isolation and culture of primary MSCs, cell treatments and phosphomimetic constructs, immunofluorescence and confocal imaging, FRAP, immunoblotting, transcriptional profiling and micropipette aspiration can be found in the Supplemental Information.

Preparation of soft and stiff hydrogel substrates

The preparation of polyacrylamide (PA) gels with controlled elasticity and covalent attachment to glass cover slips was described in detail in a published methods paper [17]; the method is also summarized in the Supplemental Information.

MS and quantification of synthetic phosphopeptides

Quantification of proteins by label-free MS is described in the Supplemental Information and earlier work [34]. MS response to phosphorylation at S22 and S390 was calibrated using synthetic versions of tryptic peptides (SGAQASSTPLSPTR, SGAQASSTPL[pSer22]PTR, LRLSPSPTSQR LRL[pSer390]PSPTSQR; GenScript), which were spiked into a tryptic cell digests (60 – 80 kDa MW band) (Fig. S1E). The data in Figs. 3C, D and S3C–E were attained without alignment between spectra (Elucidator, Rosetta Biosystems). The data in Figs. 3I, J were aligned against standards containing both phosphorylated and un-phosphorylated versions of the S22 and S390 tryptic peptides. Specificity of primary lamin-A pSer22 antibody (Rabbit polyclonal, Cell Signaling) was tested by incubation overnight at

4 °C in 3% BSA with the corresponding phospho-peptide (SGAQASSTPL[pSer22]PTR) at a peptide:Ab ratio of 10:1 (Figs. 1B; S1D).

Systems mechanobiology gene circuit

Derivations of the equations used to describe the interactions in Figure 4F are shown in the Supplementary Information and are solved in the steady state to produce the data plotted in Figures 4G and H using code written in Mathematica (Wolfram).

Supplementary Material

Refer to Web version on PubMed Central for supplementary material.

Acknowledgments

We are grateful for support from the U.S. National Institutes of Health (NIH R01HL062352; P01DK032094; R01EB007049; NCATS-8UL1TR000003), the U.S. National Science Foundation (grant 1200834), and the University of Pennsylvania's research centers (Materials Research Science and Engineering; Nano Science and Engineering; Nano/Bio Interface).

References

1. Discher DE, Janmey P, Wang YL. Tissue cells feel and respond to the stiffness of their substrate. Science. 2005; 310:1139–1143. [PubMed: 16293750]
2. Engler AJ, Sen S, Sweeney HL, Discher DE. Matrix elasticity directs stem cell lineage specification. Cell. 2006; 126:677–689. [PubMed: 16923388]
3. Levental KR, Yu H, Kass L, Lakins JN, Egeblad M, Erler JT, Fong SFT, Csiszar K, Giaccia A, Weninger W, et al. Matrix crosslinking forces tumor progression by enhancing integrin signaling. Cell. 2009; 139:891–906. [PubMed: 19931152]
4. Sawada Y, Tamada M, Dubin-Thaler BJ, Cherniavskaya O, Sakai R, Tanaka S, Sheetz MP. Force sensing by mechanical extension of the Src family kinase substrate p130Cas. Cell. 2006; 127:1015–1026. [PubMed: 17129785]
5. Even-Ram S, Doyle AD, Conti MA, Matsumoto K, Adelstein RS, Yamada KM. Myosin IIA regulates cell motility and actomyosin microtubule crosstalk. Nat Cell Biol. 2007; 9:299–U104. [PubMed: 17310241]
6. Gardel ML, Schneider IC, Aratyn-Schaus Y, Waterman CM. Mechanical integration of actin and adhesion dynamics in cell migration. Annu Rev Cell Dev Biol. 2010; 26:315–333. [PubMed: 19575647]
7. Dupont S, Morsut L, Aragona M, Enzo E, Giulitti S, Cordenonsi M, Zanconato F, Le Digabel J, Forcato M, Bicciato S, et al. Role of YAP/TAZ in mechanotransduction. Nature. 2011; 474:179–U212. [PubMed: 21654799]
8. Pelham RJ, Wang YL. Cell locomotion and focal adhesions are regulated by substrate flexibility. Proc Natl Acad Sci USA. 1997; 94:13661–13665. [PubMed: 9391082]
9. Swift J, Ivanovska IL, Buxboim A, Harada T, Dingal PCDP, Pinter J, Pajerowski JD, Spinler KR, Shin JW, Tewari M, et al. Nuclear lamin-A scales with tissue stiffness and enhances matrix-directed differentiation. Science. 2013; 341:1240104. [PubMed: 23990565]
10. Lehner CF, Stick R, Eppenberger HM, Nigg EA. Differential expression of nuclear lamin proteins during chicken development. J Cell Biol. 1987; 105:577–587. [PubMed: 3301871]
11. Dittmer T, Misteli T. The lamin protein family. Genome Biol. 2011; 12:14.
12. Schirmer EC, Florens L, Guan TL, Yates JR, Gerace L. Nuclear membrane proteins with potential disease links found by subtractive proteomics. Science. 2003; 301:1380–1382. [PubMed: 12958361]

13. Gruenbaum Y, Margalit A, Goldman RD, Shumaker DK, Wilson KL. The nuclear lamina comes of age. Nat Rev Mol Cell Biol. 2005; 6:21–31. [PubMed: 15688064]
14. Goldman RD, Gruenbaum Y, Moir RD, Shumaker DK, Spann TP. Nuclear lamins: building blocks of nuclear architecture. Genes Dev. 2002; 16:533–547. [PubMed: 11877373]
15. Heald R, McKeon F. Mutations of phosphorylation sites in lamin-A that prevent nuclear lamina disassembly in mitosis. Cell. 1990; 61:579–589. [PubMed: 2344612]
16. Ward GE, Kirschner MW. Identification of cell-cycle regulated phosphorylation sites on nuclear lamin-C. Cell. 1990; 61:561–577. [PubMed: 2188730]
17. Buxboim A, Rajagopal K, Brown AEX, Discher DE. How deeply cells feel: methods for thin gels. J Phys-Cond Mat. 2010; 22
18. Buxboim A, Ivanovska IL, Discher DE. Matrix elasticity, cytoskeletal forces and physics of the nucleus: how deeply do cells 'feel' outside and in? J Cell Sci. 2010; 123:297–308. [PubMed: 20130138]
19. Vicente-Manzanares M, Ma XF, Adelstein RS, Horwitz AR. Non-muscle myosin II takes centre stage in cell adhesion and migration. Nat Rev Mol Cell Biol. 2009; 10:778–790. [PubMed: 19851336]
20. Raab M, Swift J, Dingal PCDP, Shah P, Shin JW, Discher DE. Crawling from soft to stiff matrix polarizes the cytoskeleton and phosphoregulates myosin-II heavy chain. J Cell Biol. 2012; 199:669–683. [PubMed: 23128239]
21. Dahl KN, Engler AJ, Pajerowski JD, Discher DE. Power-law rheology of isolated nuclei with deformation mapping of nuclear substructures. Biophys J. 2005; 89:2855–2864. [PubMed: 16055543]
22. Vassilev LT, Tovar C, Chen SQ, Knezevic D, Zhao XL, Sun HM, Heimbrook DC, Chen L. Selective small-molecule inhibitor reveals critical mitotic functions of human CDK1. Proc Natl Acad Sci USA. 2006; 103:10660–10665. [PubMed: 16818887]
23. Beausoleil SA, Villen J, Gerber SA, Rush J, Gygi SP. A probability-based approach for high-throughput protein phosphorylation analysis and site localization. Nat Biotech. 2006; 24:1285–1292.
24. Dephoure N, Zhou C, Villen J, Beausoleil SA, Bakalarski CE, Elledge SJ, Gygi SP. A quantitative atlas of mitotic phosphorylation. Proc Natl Acad Sci USA. 2008; 105:10762–10767. [PubMed: 18669648]
25. Olsen JV, Vermeulen M, Santamaria A, Kumar C, Miller ML, Jensen LJ, Gnad F, Cox J, Jensen TS, Nigg EA, et al. Quantitative phosphoproteomics reveals widespread full phosphorylation site occupancy during mitosis. Sci Signal. 2010; 3:15.
26. Bertacchini J, Beretti F, Cenni V, Guida M, Gibellini F, Mediani L, Marin O, Maraldi NM, de Pol A, Lattanzi G, et al. The protein kinase Akt/PKB regulates both prelamin A degradation and Lmna gene expression. Faseb J. 2013; 27:2145–2155. [PubMed: 23430973]
27. Zastrow MS, Vlcek S, Wilson KL. Proteins that bind A-type lamins: integrating isolated clues. J Cell Sci. 2004; 117:979–987. [PubMed: 14996929]
28. Holaska JM, Kowalski AK, Wilson KL. Emerin caps the pointed end of actin filaments: Evidence for an actin cortical network at the nuclear inner membrane. Plos Biology. 2004; 2:1354–1362.
29. Ho CY, Jaalouk DE, Vartiainen MK, Lammerding J. Lamin A/C and emerin regulate MKL1-SRF activity by modulating actin dynamics. Nature. 2013; 497:507–511. [PubMed: 23644458]
30. Olson EN, Nordheim A. Linking actin dynamics and gene transcription to drive cellular motile functions. Nat Rev Mol Cell Biol. 2010; 11:353–365. [PubMed: 20414257]
31. Sullivan T, Escalante-Alcalde D, Bhatt H, Anver M, Bhat N, Nagashima K, Stewart CL, Burke B. Loss of A-type lamin expression compromises nuclear envelope integrity leading to muscular dystrophy. J Cell Biol. 1999; 147:913–919. [PubMed: 10579712]
32. Kubben N, Voncken JW, Konings G, van Weeghel M, van den Hoogenhof MMG, Gijbels M, van Erk A, Schoonderwoerd K, van den Bosch B, Dahlmans V, et al. Post-natal myogenic and adipogenic developmental defects and metabolic impairment upon loss of A-type lamins. Nucleus. 2011; 2:195–207. [PubMed: 21818413]

33. Schwanhausser B, Busse D, Li N, Dittmar G, Schuchhardt J, Wolf J, Chen W, Selbach M. Global quantification of mammalian gene expression control. Nature. 2011; 473:337–342. [PubMed: 21593866]

34. Swift J, Harada T, Buxboim A, Shin JW, Tang HY, Speicher DW, Discher DE. Label-free mass spectrometry exploits dozens of detected peptides to quantify lamins in wildtype and knockdown cells. Nucleus. 2013; 4:7–6.

Highlights

- MSCs on soft matrix exhibit a less spread nucleus with low lamin-A,C levels.
- Lamin-A,C is rapidly phosphorylated in response to reduced cytoskeletal tension.
- Phosphorylation leads to nuclear softening and lamin-A,C turnover.
- Levels of lamin-A,C and myosin-IIA are co-regulated in response to matrix elasticity.

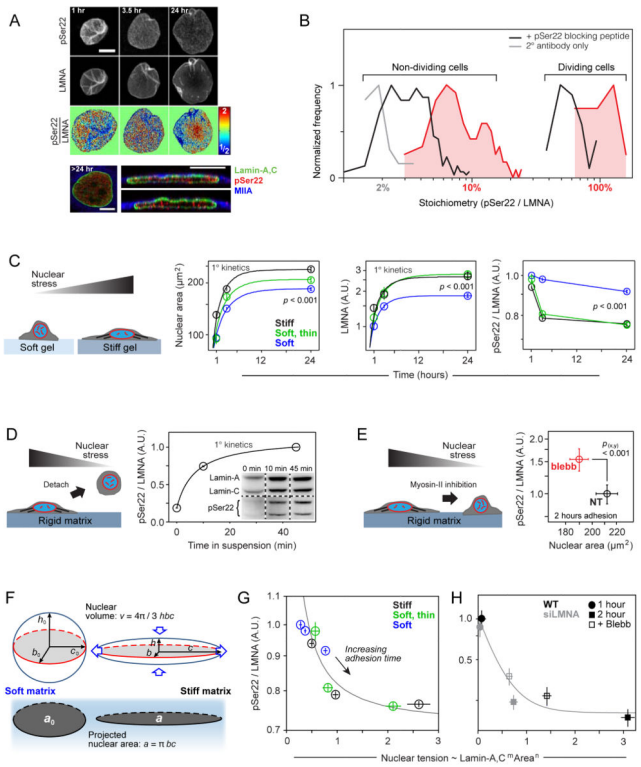

Figure 1. Increased stress on the nucleus suppresses lamin-A,C phosphorylation

(**A**) Lamin-A,C pSer22 is present in interphase cells. Top two rows: confocal image stacks of total and pSer22 lamin-A,C in MSCs fixed after 1-to-24 hours of adhesion showed wrinkled nuclei at early stages of cell adhesion that stretched and smoothed with spreading. Third row: pSer22/LMNA ratios from the top two panels, calculated pixel-by-pixel and normalized to mean fold-change. After 24 hrs, greater phospho-LMNA concentration was observed in the nucleoplasm vs. at the nuclear periphery. Bottom row: Confocal cross-sections confirmed nucleoplasmic pSer22 (all scale bars = 10 μm).

(**B**) Histogram of pSer22 levels in a population of A549 cells (Figs. S1A–D), showing specificity of pSer22 immunofluorescence and stoichiometry calibrated by MS (Fig. S1E). Dividing cells showed the greatest extent of phosphorylation (Fig. S1C). Pre-incubation with a phospho-epitope blocking peptide decreased immunofluorescence intensity, as did non-specific binding to a non-phosphorylated version of the same peptide, but to a significantly lesser extent (Fig. S1D). In the absence of primary antibody (2° antibody only), fluorescence intensity was very low (n = 33–249 cells per group).

(**C**) Stiff matrix enhances nuclear stress which inhibits phosphorylation of lamin-A,C. Stress on nuclei in MSCs was manipulated by changing matrix stiffness and adhesion time. Cells spread, with correspondingly greater projected nuclear areas, with increasing adhesion time, and to a greater extent on stiff (40 kPa, black line) vs. soft (0.3 kPa, blue line) substrate. A thin, soft matrix (0.3 kPa, green line) showed behavior intermediate between soft and stiff. The matrix-modulated adhesion process was accompanied by an increase in the total LMNA and a reduction in the fraction pSer22/LMNA. Error bars in all plots show ± SEM (n = 77–276 cells per group).

(**D**) Cell detachment increased pSer22/LMNA in rounding nuclei, with phosphorylation (quantified by immunoblot; $n = 3$) increasing over tens of minutes in suspension, consistent with relaxation of nuclear stress.
(**E**) pSer22/LMNA increased with myosin-IIA inhibition and stress relaxation by blebbistatin (blebb) treatment (immunofluorescence, Fig. S1E) ($n = 25–32$ cells per group).
(**F**) Nuclear shape was modeled as an ellipsoid, with surface area assumed to be constant during nuclear deformation. During cell spreading, the nucleus was stretched and flattened down against the substrate, subject to tangential stretching ('hoop strain') but negligible radial strain. As the hoop strain scaled with the radius r, and the fold-change in r can be estimated by the square root of the fold-change in projected nuclear area, we concluded that the nuclear strain involved in cell spreading can be estimated by $\varepsilon \sim \sqrt{a/a_0}$, where a is the nuclear projected area and a_0 corresponds to the initial state.
(**G**) By expressing nuclear tension as a function of lamin-A,C level and nuclear area, pSer22/LMNA data was fit to hyperbolic decays. Plot shows data fitting for MSCs cultured on soft, soft/thin and stiff hydrogel substrates (adhesion time: 1, 3.5 and 24 hrs; Fig. 1C).
(**H**) Data fitting for MSCs subjected to lamin-A,C KD and blebbistatin treatment (Figs. 1E; S1E).

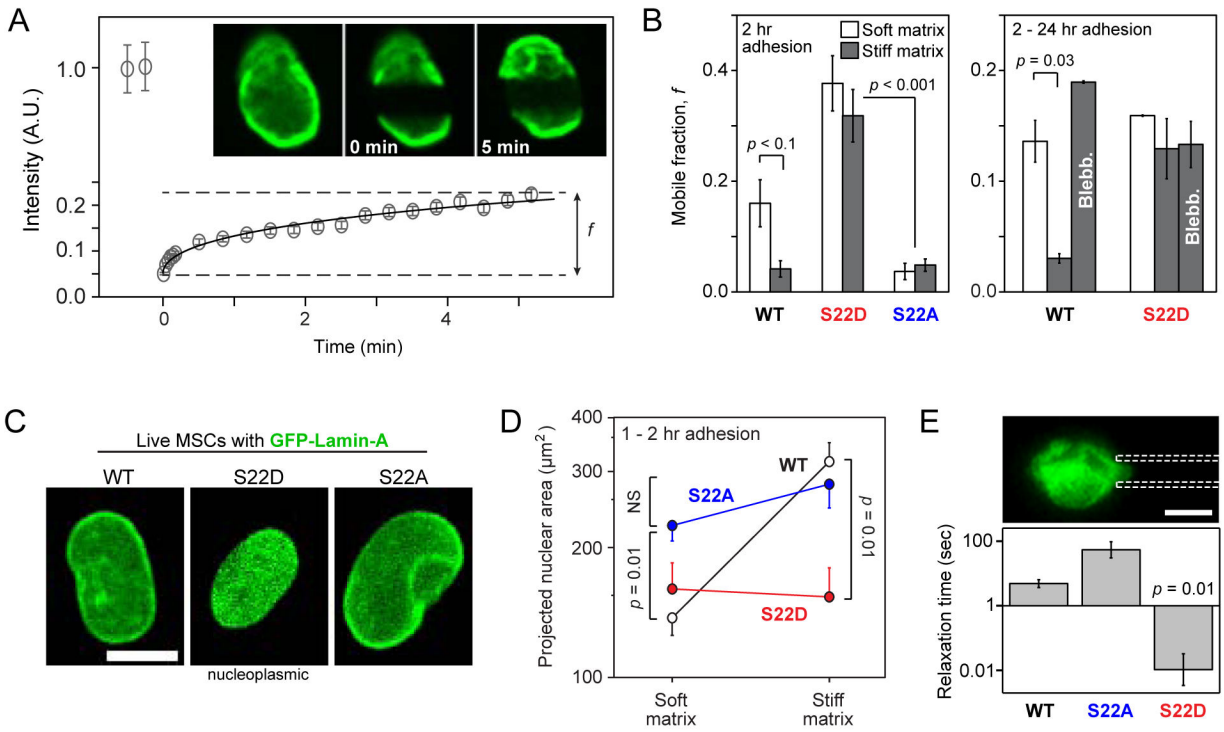

Figure 2. Phosphomimetic lamin-A constructs show increased mobility and soften the nucleus

(**A**) The mobile fraction, *f*, of GFP-fused wild-type lamin-A and phosphomutant lamin-A constructs (S22D and S22A) was evaluated by fitting an exponential curve to the recovering intensities of wide side-to-side bands photobleached in the nuclei of MSCs.

(**B**) Analysis of FRAP experiments showed that the WT construct was comparatively more mobile in MSCs cultured for 2 hrs on soft (0.3 kPa) than on stiff (40 kPa) substrate (Fig. S2A). Independent of matrix stiffness, S22D mobile fractions were higher than WT, whereas S22A remained polymerized (Fig. S2B). WT lamin-A was solubilized by blebb after 24 hours on stiff gels, but treatment of phosphomimetic S22D showed no significant change (*n* = 9–18 nuclei per group).

(**C**) Live-cell imaging of WT, S22D and S22A phospho-mimetic GFP-lamin-A constructs. S22D showed a diffusive nucleoplasmic distribution and low nuclear spreading, consistent with a nucleoplasmic distribution of pSer22.

(**D**) S22D and S22A suppressed matrix mechanosensitivity of MSCs whereas WT nuclei spread by > 2-fold on stiff matrix (40 kPa) relative to soft matrix (0.3 kPa) (*n* = 5–18 nuclei per group).

(**E**) Relaxation times measured by micropipette aspiration showed S22D nuclei to be significantly softer than WT nuclei, and S22A nuclei were moderately stiffer. Relaxation times were determined at the same value of creep compliance ($J = 1.4\ \text{kPa}^{-1}$) per [21]. Error bars show log mean ± SEM (*n* > 4 nuclei).

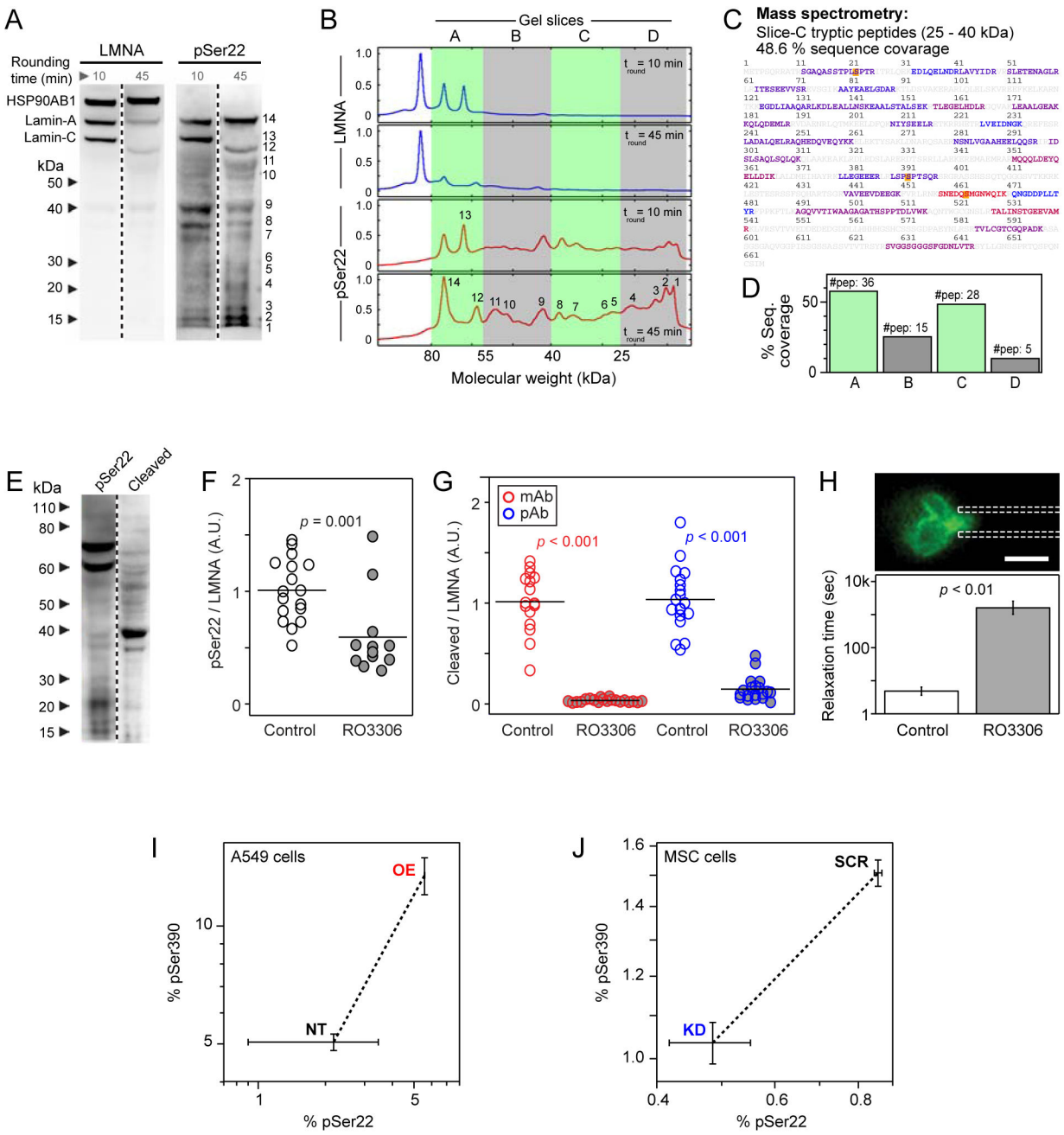

Figure 3. Phosphorylation of lamin-A,C promotes proteolysis and nuclear softening

(**A**) Phospho-lamin-A,C is present in both full-length and cleaved states. MSCs lysed following short (10 min) and long (45 min) periods of rounding in suspension showed numerous low-MW, fragmentation-product bands in immunoblots against lamin-A,C and, to a greater extent, against pSer22.

(**B**) Profiles of immunoblots, showing MW ranges analyzed by MS (densitometry shown in Figs. S3A, B).

(**C**) Gel slices A-to-D were analyzed by MS, confirming the existence of low MW lamin-A cleavage products (peptide coverage of 25 – 40 kDa range shown; blue-to-red coloring

indicates peptides detected with increased ion current). Phosphorylation sites detectable by MS are indicated in yellow.

(**D**) All examined bands had lamin-A fragments (see Fig. S3C for sequence coverage maps).

(**E**) Inhibition of lamin-A,C phosphorylation suppresses cleavage. Immunoblots against lamin-A pSer22 or lamin-A cleavage product(s). The latter antibody shows minimal detection of intact lamin-A and a high intensity band at 40 kDa.

(**F**) Treatment with CDK inhibitor RO3306 reduced the extent of phosphorylation at Ser22 in MSCs.

(**G**) RO3306 also suppressed the formation of lamin-A,C cleavage products, as determined by two independent antibodies (see Figs. S3F–H for representative images and analysis).

(**H**) Drug induced lamin-A,C phospho-inhibition stiffened the nucleus as determined by micropipette aspiration (relaxation times determined at constant compliance, $J = 1.25\ \mathrm{kPa}^{-1}$ per [21]). Error bars show log mean ± SEM ($n > 4$ nuclei).

(**I**) MS showed a correlated increase in phosphorylation at S22 and S390 during lamin-A overexpression in A549 cells.

(**J**) Phosphorylation at S22 and S390 showed a correlated decrease during lamin-A,C KD in MSCs (error bars show ± SEM; see Fig. S1D for calibration of phosphorylation measurements by MS).

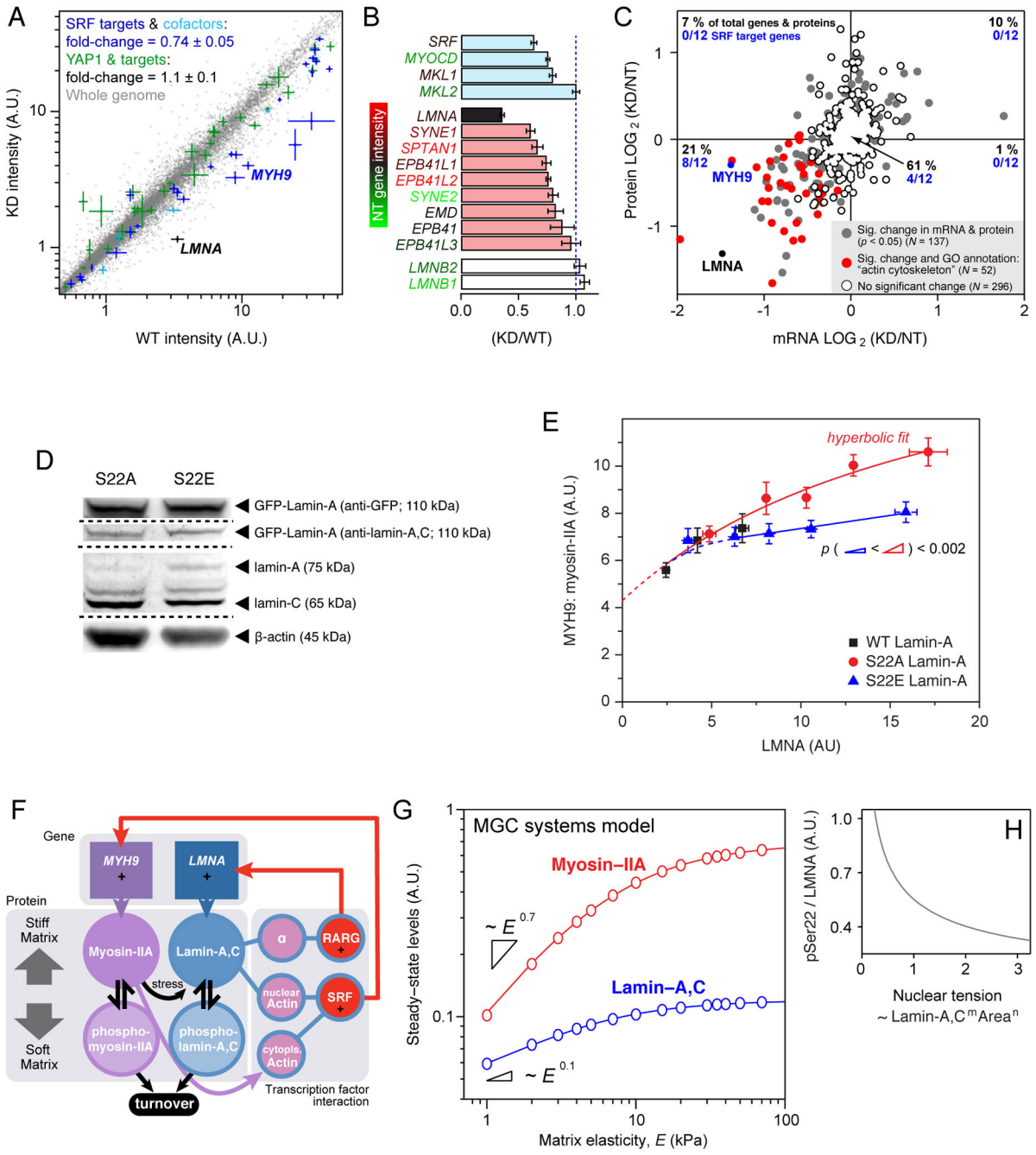

Figure 4. Lamin-A,C level and phosphorylation state regulate myosin-IIA, factors that can be combined into a mechano-sensitive gene circuit model

(**A**) Lamin-A,C level regulates myosin-IIA through the Serum Response Factor (SRF) pathway. Transcriptional profiling of MSCs subjected to lamin-A,C KD (n = 3). SRF and cofactors (in cyan) and target genes (blue) were significantly suppressed. The YAP1-regulated Hippo pathway has also been implicated in cellular mechanosensitivity [7], but appeared unaffected here.

(**B**) Transcripts of SRF and cofactors (cyan) were suppressed with lamin-A,C KD, along with those of multiple actin-binding nuclear envelope proteins (red) ($n = 3$) (see Fig. S4A for GO-term analysis).

(**C**) Correlation between protein and transcript changes with lamin-A,C KD in MSCs. Points represent 485 proteins quantified by MS with three-or-more peptides per protein, and their associated mRNA quantified by DNA microarray. Each point is averaged from three biological replicates and the genes/proteins that are significantly perturbed ($p < 0.05$) counted in the four quadrants of the plot. Of genes with GO annotation "actin cytoskeleton", ($n = 52$, in red), 14 are unchanged and 36 have reduced levels of protein and mRNA. Of genes classified as SRF targets ($n = 12$) by Olson et al, four are unchanged and eight – including myosin-IIA (*MYH9*) – have reduced levels of protein and mRNA [30].

(**D**) S22A and E GFP-lamin mutants expressed in cells with knockdown of endogenous lamin-A,C show roughly similar levels of both constructs and endogenous protein.

(**E**) Lamin-A,C phosphorylation feeds back into myosin-IIA level. Expression of increasing levels of phosphomimetic GFP-S22E-lamin-A in A549 cells with KD of endogenous lamin-A,C had minimal effect on myosin-IIA levels. In contrast, expression of an non-phosphorylatable S22A construct caused a relatively increased quantity of myosin-IIA (x-axis shows total LMNA; S22A data fit by hyperbolic function: $y = abx\,(1 + bx)^{-1} + c$ ($a = 1.3$; $b = 5.5$; $c = 4.3$; $R^2 > 0.95$); each point is averaged data from $n > 20$ cells; see Figs. S4B–D for representative images and analysis of cell morphology).

(**F**) Tension dependent phosphorylation and turnover feeds into transcriptional regulation, as captured by a *Mechanobiological Gene Circuit (MGC) systems* model that couples both lamin-A,C and myosin-IIA levels to matrix stiffness. Lamin-A,C transcriptionally regulates *LMNA* via the retinoic acid pathway (through a mediator, α) and also *MYH9* via the SRF pathway through nuclear actin. On stiff matrix, non-phosphorylated, contraction-competent myosins positively regulate lamin-A,C favoring assembly and opposing degradation that occurs on soft matrices.

(**G**) The MGC systems model predicted that lamin-A,C and myosin-IIA levels should monotonically increase with matrix elasticity but also saturate on rigid substrates.

(**H**) MGC model suggests decreased lamin phosphorylation with increasing nuclear tension (consistent with model and experimental data shown in Figs. 1F–H).